

## T.1: Photonic nanojet: generation, manipulation and applications

H. S. Patel and S. K. Majumder

Laser Biomedical Applications Section

Email: harish@rrcat.gov.in

### Abstract

Photonic nanojets, because of their ability to confine electromagnetic waves in sub wavelength scale dimension, have emerged as a useful aid in high resolution imaging and spectroscopy applications. In this article, we review the different approaches used for generation and controlled manipulation of photonic nanojets. We also provide a summary of various applications being explored using photonic nanojets.

### 1. Introduction

Confinement of light to sub-wavelength dimensions is limited by diffraction criteria that prevent ultimate spot size to approximately half the wavelength of the illuminating radiation. A number of techniques will immensely benefit if the light can be localized beyond the diffraction limit since such a capability will allow high resolution imaging as well as fabrication, characterization and manipulation of materials with nano meter scale dimensions. One approach for improving the resolution is to use waves of shorter wavelengths for imaging. This has led to the development of UV and x-ray microscopy techniques that use electromagnetic waves with a shorter wavelength than visible light. However, lack of high brightness source at these wavelengths coupled with strong absorption of UV in conventional glass materials and difficulty in focusing of the x-ray make these systems complicated and expensive. The electron microscope that makes use of electron beam also facilitates imaging with higher spatial resolution as the de Broglie wavelength of accelerated electrons is significantly smaller compared to UV / x-ray and hence lowers the diffraction limit. The electron microscope however, requires high vacuum and considerable sample preparation (to avoid space charge effect) making them unsuitable for imaging of live samples. There has been a persistent effort by scientific community to develop techniques for imaging live cells and biological processes in their native environment. A number of far-field microscopy techniques have been developed to overcome the resolution limit set by diffraction criteria [1-3]. These include stimulated emission depletion microscopy [4], photo-activated localization microscopy [5], stochastic optical reconstruction microscopy [6] and the structured-illumination microscopy [7] etc. However, these techniques require use of suitable fluorescent labels with stringent

characteristics to achieve the super resolution imaging. Near-field optics that deals with the non-propagating evanescent field existing near the surface of an object at distances less than a single wavelength of illumination light provides an alternative approach to achieve resolution much smaller than the wavelength. The near-field scanning optical microscope (NSOM) that uses optical near-field for the imaging and spectroscopy has emerged as one of the important optical tools for characterization of features having sub-wavelength dimensions [8]. One of the main problems in such near-field optical tools, however, is that the signal intensity in the near field is extremely weak. This is because of the fact that the tapered fibre probe or a hollow cantilever type probe used in a conventional NSOM for confining the light to sub-diffraction spot has extremely low throughput that decreases rapidly with the decrease in aperture size [9]. Throughput of these probes for visible light illumination is generally  $\sim 10^{-4}$ . Thus, from 1 mW input power, which is the typical power handling capacity of these probes, one can expect to get only  $\sim 100$  nW power at the tip apex. While it may be sufficient for high resolution imaging and near field photoluminescence measurements, many applications like near field Raman scattering, high density optical recording of data, and nanolithography etc. require significantly higher power at the sample. Further, the tightly confined field at the spot size of sub-wavelength scale comes at the price of a very fast divergence of the beam. This has prompted researchers across the globe to develop alternative approaches to alleviate these problems associated with near field signal. One approach that has received considerable attention in the past decade is the use of photonic nanojet (PNJ) for generating highly confined electromagnetic field on the sub-wavelength scale. A PNJ is generated when a transparent dielectric micro-particle of appropriate size and refractive index is illuminated with an electromagnetic wave. In this article, we first discuss the techniques used for generation and controlled manipulation of photonic nanojet characteristics. This will be followed by a brief summary of various applications being explored using photonic nanojet.

### 2. Generation of photonic nanojet

Existence of high intensity region with sub-diffraction lateral confinement was first predicted by Chen *et al.* [10] in the year 2004 with the help of numerical simulation of electromagnetic field in and around the transparent dielectric microsphere illuminated with plane wave. The formation of high intensity region near the shadow surface of a microsphere can be traced back to Barton *et al.* [11] who demonstrated strong localization of the electric field near the surface of 5  $\mu\text{m}$  diameter water droplet in air upon excitation with a focused Gaussian beam. The term "photonic nanojet" was first coined and its detail characteristics were

investigated by Chen *et al.* [10]. Subsequently, the near field focusing effects and jet like structure were observed by a number of investigators [12-16]. Micron size dielectric particles of a variety of different sizes, shapes and refractive indices have been explored for generating PNJ of desired characteristics. Figure T.1.1 shows a typical intensity distribution in the photonic nanojet generated by a silica microsphere under plane wave illumination. The first experimental evidence of the existence of PNJ came from the study of Kong *et al.* [17] wherein the reading of data from sub-wavelength sized pits was demonstrated using nanojet of microwave radiation. It was followed by experimental observation of PNJ generated by dielectric microsphere using confocal imaging under visible light illumination by Ferrand *et al.* [18]. Unlike the whispering gallery modes, generation of PNJ is not a resonance phenomenon and has been shown to be relatively insensitive to the deformation and surface corrugations [19, 20] and hence can be observed for a wide range of diameters of the micro-particles and wavelength of the illumination, provided the relative refractive index contrast with respect to the background is less than approximately 2:1 [21].

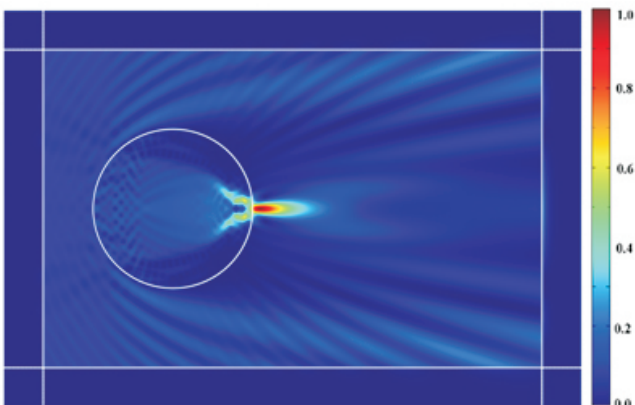


Fig. T.1.1: Normalized intensity distribution in a typical photonic nanojet generated by microsphere of diameter  $4 \mu\text{m}$  at incident wavelengths of  $514 \text{ nm}$ . Refractive index of the microsphere is  $n_s = 1.59$  and that of the surrounding medium is  $n_o = 1.0$ .

### 2.1 PNJ characteristics

Photonic nanojet has significant contribution from the optical near field generated at the exit surface of the beam. This leads to confinement of the field beyond the limit of diffraction and shows exquisite characteristics that depends on the material properties and geometry of the micro-particle, surrounding environments and illumination wavelength. Key parameters of PNJ that determine the choice of micro-particles for a given application are jet length, jet width, peak intensity and the working distance. Figure T.1.2 shows a pictorial depiction of

these parameters for a typical PNJ.

The length of a PNJ is defined as the distance from the edge of the sphere to a point along the optic axis where the intensity drops to twice that of the incident light. Typically with a homogeneous microsphere geometry, PNJ length of  $\sim 3\lambda$  can be realized. Further increase in the length has been demonstrated by immersing the microsphere in a liquid environment [22], using microsphere with concentric or axially eccentric shells of graded refractive indices [23] and via shaping of the incident wavefront [24]. However, it is important to note here that the longer PNJs are often accompanied with poor lateral confinement and reduced peak intensity.

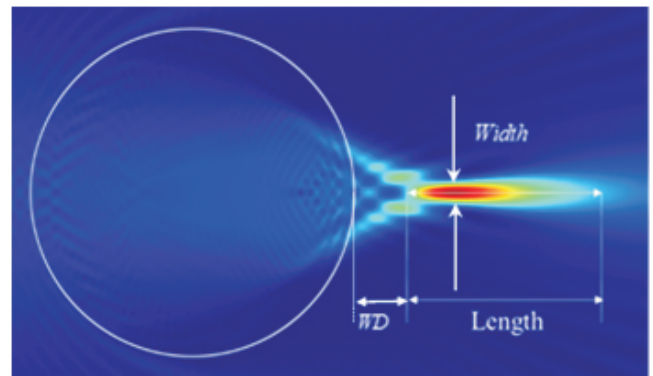


Fig.T.1.2: Pictorial depiction of photonic nanojet parameters.

The width of a PNJ is defined as full width at half maxima (FWHM) of the transverse intensity profile measured at highest intensity along the optic axis. Typical width of PNJ is  $\sim 0.4\lambda$  for microspheres having refractive index of 1.45 (Figure T.1.2). The width of PNJ depends strongly on the refractive index of the micro-particles and reduces with increase in the refractive index till its refractive index contrast with the surrounding is less than 2. Further increase in the refractive index of the particle leads to a PNJ that has peak intensity point located inside the micro-particle. It is for this reason that both the width and the length of a PNJ are measured at the point lying outside the shadow surface of micro-particle.

The peak intensity of a PNJ is generally expressed in terms of the normalized intensity at the maxima in axial intensity profile of the PNJ with respect to the incident beam intensity and hence denotes enhancement in the intensity due to localization of field in the nanojet. Relative peak intensity of  $\sim 150$  has been reported in the literature using silica microsphere.

The working distance of a PNJ is another parameter that plays an important role in determining the ability to examine samples through thicker interfaces such as nanoparticles migrating inside the biological cells. The working distance of a PNJ is defined as the distance from micro-particle surface to the maximum intensity point in a PNJ from on shadow side of the particle.

### 3. Manipulation techniques for tailoring PNJ characteristics

Because of their ability to confine the light in sub-wavelength spatial dimension, PNJ is rapidly emerging as a simple and cost effective approach for localized illumination/collection of scattered light with rich near field information for high resolution imaging and spectroscopy. Some of the important areas in which PNJs offer subtle advantages is enhancement of Raman signal [25,26], single molecule spectroscopy [27], fluorescence correlation spectroscopy [28], nano photolithography [29-31] and nanoscopy [32,33] etc. Effective utilization of PNJ for many of these applications requires precise control over its characteristics to achieve optimal performance. Therefore, during last decade a considerable research effort has been directed towards tailoring of PNJs either for better confinement and thus higher peak intensity or for elongation of nanojet for high resolution far field applications. Several approaches have been proposed for manipulating the length and confinement of photonic jet. The results reported in literature show that the length and full width at half maxima (FWHM) of photonic nanojet depend on size and shape of micro particle, refractive index of particle and that of the surrounding medium, wavelength, polarization and beam profile of the excitation light etc. Apart from conventional shapes like sphere and cylinder, particles of other shapes such as axicon, micro cuboids, micro disks, concentric graded index microsphere or ellipsoids, core-shell microspheres and truncated microspheres etc. have also been explored in various studies to investigate tuning of PNJ characteristics [34]. More recently, Eti *et al.* [35] have demonstrated controlled manipulation of photonic nanojet by tuning the refractive index in liquid crystals filled micro shells.

Techniques used for manipulation of PNJ characteristics can be broadly classified into two categories. First, that deals with morphology of the particle wherein the size, shape, and refractive index profile of the particle and surrounding medium is varied to tailor the PNJ characteristics. The second approach uses variation in the beam parameter such as convergence/divergence of the beam, beam profile, wavelength and polarization etc. to engineer the nanojet.

### 3.1 Manipulation using particle morphology

#### 3.1.1 Size dependence of PNJ characteristics

Size of the microsphere plays an important role in determining the characteristics of PNJ generated by micro-particles. PNJ has been reported for microspheres of sizes ranging from about a wavelength to  $30\lambda$ . However, as the size of microsphere increases, the lateral confinement of PNJ becomes poorer and gradually approaches that predicted by the geometric optic approximation for larger size microsphere and no longer serves the purpose of sub-diffraction confinement. Figure T.1.3 shows the effect of microsphere size on the axial length and lateral confinement of PNJ generated by silica microsphere ( $n_s = 1.45$ ) placed in air ( $n_o = 1.0$ ) under plane wave illumination with 500 nm wavelength. It can be seen from figure that sub-diffraction ( $\sim \lambda/2$ ) lateral confinement is maintained for microspheres of sizes less than  $\sim 3 \mu\text{m}$ . As the size of microsphere reduces both the length and the width of the PNJ decreases which leads to higher peak intensity in the nanojet. For microsphere of size smaller than  $0.5 \mu\text{m}$  radius, the peak intensity in the nanojet lies inside the microsphere due to higher curvature seen by the light falling on the microsphere surface. This effectively leads to an increase in the width of PNJ emerging on the shadow side of the microsphere.

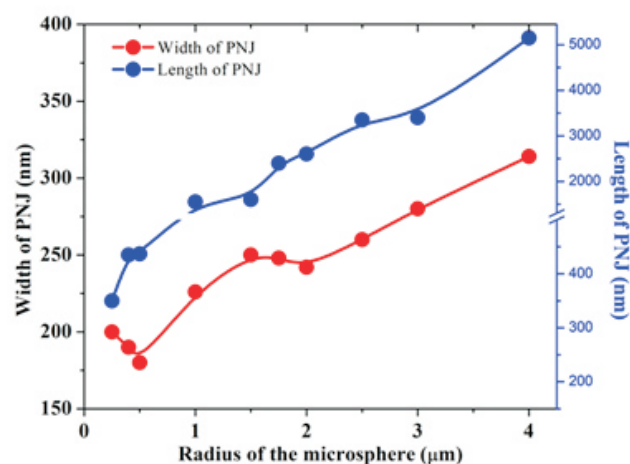


Fig. T.1.3: Length and width of PNJ as a function of the microsphere radius. Illumination wavelength is 500 nm, silica microsphere ( $n_s = 1.45$ ) was placed in air.

#### 3.1.2 Manipulation through refractive index variation

Dependence of PNJ characteristics on the refractive index of the particle was systematically investigated using numerical simulations for microsphere of  $3 \mu\text{m}$  diameter while varying the refractive index ' $n_s$ ' of microsphere from 1.3 to 2.0. A



typical intensity distribution in the photonic nanojet for particle with refractive index 1.7 is shown in Figure T.1.4 along with the variation of FWHM as a function of refractive index of micro-sphere. As the refractive index of microsphere increases, FWHM of photonic nanojet generated by microsphere decreases due to sharper bending of the photons

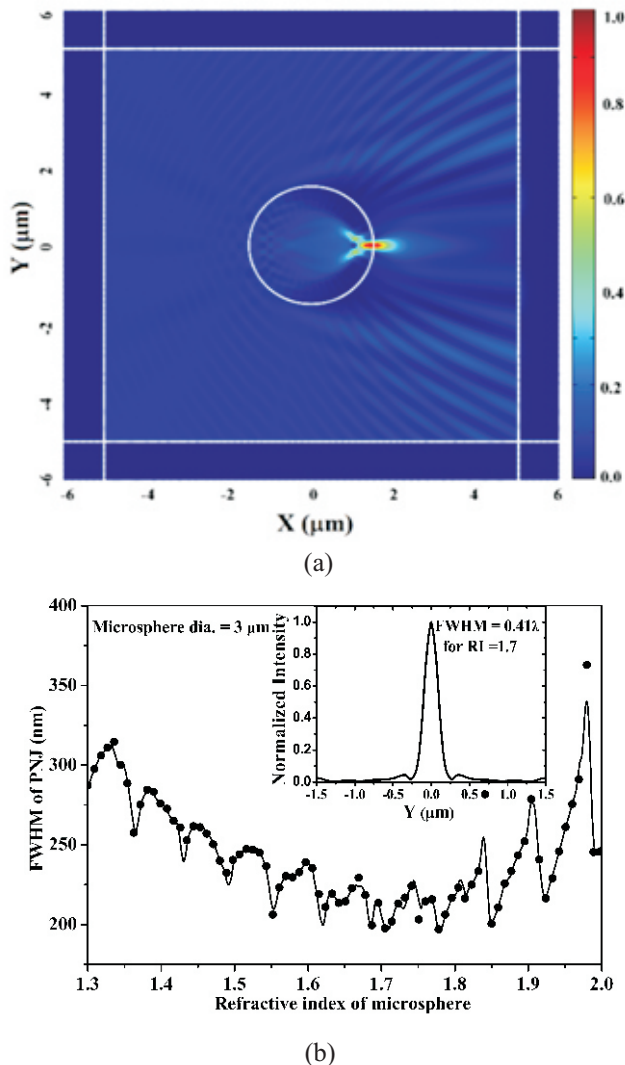


Fig.T.1.4: (a) A typical intensity distribution generated by  $3 \mu\text{m}$  microsphere ( $n = 1.7$ ) illuminated with  $500 \text{ nm}$  excitation wavelength and (b) variation of FWHM of PNJ as a function of refractive index of microsphere (bottom). The inset on right panel shows the transverse intensity profile of the nanojet formed by microsphere having refractive index 1.7 [reproduced with permission from Ref. 23].

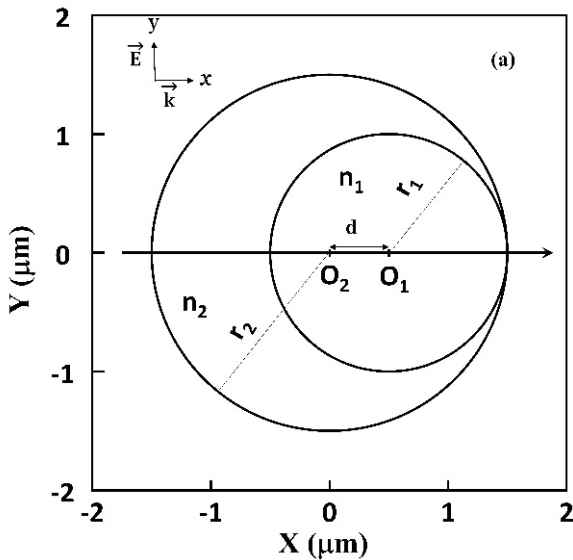
at curved surfaces of microsphere resulting in a better confinement. The smallest FWHM achieved was  $204 \text{ nm}$  corresponding to the refractive index 1.7. Further increase in the refractive index leads to the formation of PNJ that has peak intensity inside the microsphere. Thus the usable PNJ protruding outside the microsphere have larger FWHM. The transverse profile of nano jet (along the  $y$ -axis) at peak intensity point for microsphere having refractive index 1.7 is shown in the inset plot.

It should be noted here that maximum refractive index for which PNJ peak lies on or beyond the microsphere surface on shadow side reduces with decrease in size of the microsphere. PNJ is also highly sensitive to the change in refractive index of the surrounding medium which can also be used for controlled manipulation of its characteristic. A highly elongated PNJ with length exceeding  $100 \lambda$  has been reported with cylindrical micro particle immersed in liquid [22]. The liquid immersion of microsphere has also been shown to improve the resolution of microsphere nanoscopy. With a suitable choice of size and the ratio of the refractive indices of sphere with that of the surrounding medium it is possible to control the peak amplitude and decay length of the nanojet. Using the simulation results Ding *et al.* demonstrated that peak intensity in the PNJ increases with increasing refractive index of the surrounding [36]. However, the decay length and the lateral confinement of PNJ decrease with the increasing refractive index of the surrounding. Effect of coating layer on PNJ characteristics of microsphere coated with thin layer of dielectric material having different optical properties has also been investigated and shown to modify the PNJ characteristics. A simple two-component core-shell structure comprising an inclusion microsphere (the core) inside a host microsphere (shell), is one of the simplest approach that has been investigated extensively for their ability to generate enhanced field in the vicinity of laser illuminated coated microsphere.

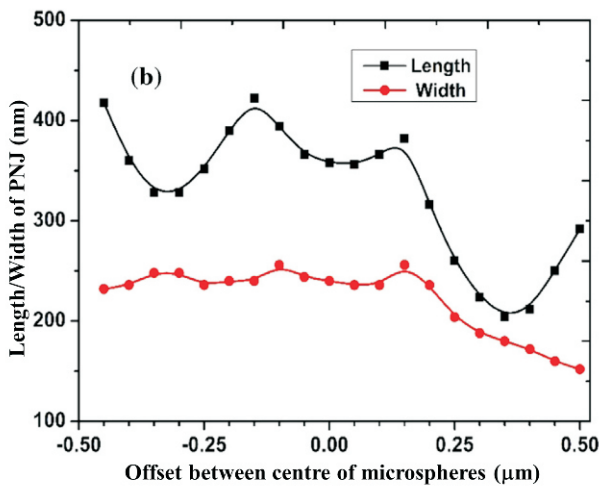
### 3.1.3 Manipulation of PNJ using core-shell microsphere

Though the characteristics of PNJ generated by dielectric microsphere can be altered by changing size, shape and refractive index, tuning in PNJ parameters is possible only over a limited range. A core-shell structure comprising two layer microspheres can provide additional control for manipulation of nanojet characteristics through change in refractive indices and separation between the centres of constituent microspheres. We have, therefore, explored the possibility of using core-shell microsphere for manipulation of PNJ characteristics. A schematic of the core shell microsphere geometry considered in simulation is shown in Figure T.1.5. The diameter of the core and shell were taken as

3  $\mu\text{m}$  and 2  $\mu\text{m}$  respectively. The core ( $n_c$ ) and shell ( $n_s$ ) refractive index was taken as 1.7 and 1.3 and the separation between core and shell centre was varied from  $-0.5 \mu\text{m}$  to  $+0.5 \mu\text{m}$  in steps of  $0.05 \mu\text{m}$  along the direction of propagation which is also the symmetry axis.



(a)



(b)

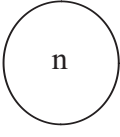
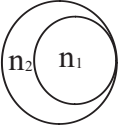

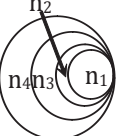
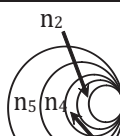
Fig. T.1.5: (a) The geometry of micro-sphere used in the simulation and (b) the FWHM (redline with circle symbol) and length (black line with square symbol) of PNJ generated by two eccentric microspheres having refractive index 1.7 (inner microsphere) and 1.3 (outer microsphere) [23].

The incident plane wave was considered to be propagating in the 'x' direction with TM polarization as shown in Figure T.1.5(a). The origin of the coordinate system was chosen to be at the centre of the shell microsphere. The length and width of nanojet for different offset positions are shown in Figure T.1.5(b). It can be seen that the length of nanojet increases when core is moved away from the centre along the direction opposite to the incident beam ( $-x$  axis). Moving the core centre in beam direction leads to shortening of the nanojet length. The maximum elongation in the length of the nanojet is obtained when the core centre is offset by approximately  $-0.5 \mu\text{m}$  from the shell centre whereas best confinement is achieved when the core centre is offset by  $+0.5 \mu\text{m}$  forming a crescent structure as shown in Figure T.1.5(a).

Simulations were also carried out to investigate the effect of interchanging refractive index of core and shell microsphere on characteristics of PNJ. While the lateral confinement of nanojet and peak intensity was found to be higher when core refractive index is higher than the shell refractive index i.e.  $n_c > n_s$ , the length of nanojet was found to be longer when  $n_s > n_c$ .

Kong *et al.* have carried out simulation for PNJ generated by 2  $\mu\text{m}$  diameter microsphere comprising up to 200-shells of 5nm thickness each to form a graded-index microsphere [13]. The microsphere refractive index profile was such that the refractive index decreases linearly in the radial direction and approaches to unity at the edge starting from  $n = 2$  at the core. The result show that the graded-index microsphere generates a significantly elongated PNJ in the propagation direction. While the generation of highly elongated PNJs is relatively easy, generating a highly confined PNJ is challenging. The core-shell microsphere was found to provide best lateral confinement when the inclusion microsphere touches the surface of the shell at the point of emission of nanojet forming a crescent shaped refractive index profile in the microsphere i.e. when the centres of two microspheres are separated by  $d \sim r_2 - r_1$ . We carried out systematic investigation of the effect of multi-layer crescent shape refractive index profile (CSR) with a goal to generate PNJ with best possible lateral confinement. Numerical simulations were performed by introducing microsphere of varying refractive indices in the range 1.3 to 2.1 into the crescent shape microsphere. The constraint that is applied to the refractive indices of different layer is that outer microsphere should have lower refractive index than the inclusion microsphere. Table T.1.1 summarizes the result obtained for multilayer microspheres of different refractive index profile.

Table T.1.1: Properties of PNJ generated by CSRP microspheres upon illumination with 500 nm wavelength in free space [23].

Design of microsphere	Refractive indices of different layers	Diameter of different layers (μm)	FWH of PNJ (nm)
	$n = 1.7$	3.0	204
	$n_1 = 1.7, n_2 = 1.3,$	$d_1 = 2.0, d_2 = 3.0,$	152
	$n_1 = 1.9, n_2 = 1.6, n_3 = 1.3,$	$d_1 = 1.0, d_2 = 2.0, d_3 = 3.0,$	140
	$n_1 = 2.0, n_2 = 1.7, n_3 = 1.6, n_4 = 1.3,$	$d_1 = 0.5, d_2 = 1.0, d_3 = 2.0, d_4 = 3.0,$	128
	$n_1 = 2.1, n_2 = 1.8, n_3 = 1.7, n_4 = 1.6, n_5 = 1.3,$	$d_1 = 0.25, d_2 = 0.5, d_3 = 1.0, d_4 = 2.0, d_5 = 3.0,$	110

### 3.1.4 Shape controlled manipulation of PNJ

It is well known fact that in the geometric optic approximation focal point of the microsphere lens (radius 'a' and refractive index  $n_p$ ) placed in air is located at [37]

$$f = \frac{a}{2} \left( \frac{n_p}{n_p - 1} \right) \quad (1)$$

from the microsphere centre. It can be seen from the above expression that for refractive index  $n_p > 2$ , focal point lies within the lens. Similar observations have been reported in the

literature for PNJ generated by microsphere. For a given size of microsphere, peak intensity in the PNJ is localized inside the microsphere when refractive index increases beyond a certain value. This is because of high positive curvature acquired by the wave front passing through the particle leading to focusing of the light within the microsphere. It is therefore expected that if the microsphere is sheared at appropriate distance from the centre, one can get PNJ with usable working distance even with higher refractive index materials thereby significantly increasing the range of

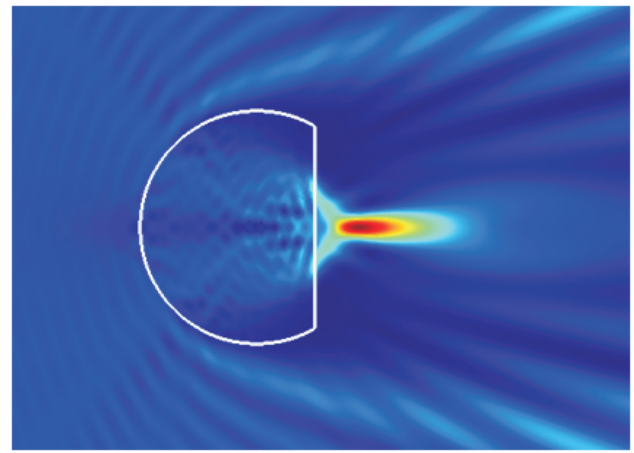


Fig.T.1.6: Intensity map of PNJ generated by sheared micro-cylinder. Refractive index of cylinder was taken as 1.59 and that of surrounding as 1.0. The incident light having wavelength of 488 nm propagates from left to right. A 3 μm diameter circular cylinder was sheared at a distance of 0.75 μm away from the long axis.

materials available for generating PNJ. Liu *et al.* investigated the effect of truncated microsphere generated by shearing the particle at different cutting thickness [38]. The photonic nanojets formed by the sheared non-spherical micro-particles with different cutting thicknesses allow controlled modulation of the axial and transverse profiles of photonic nanojet. Figure T.1.6 shows intensity map of nanojet generated by infinite micro-cylinder with non-circular cross-section fabricated by shearing the circular cylinder with 3 μm diameter at a distance of 0.75 μm from the long axis. The refractive index of cylinder was taken as 1.59 and that of surrounding as 1.0. The incident light having wavelength of 488 nm propagates from left to right. It can be seen from the figure that it is possible to manipulate the working distance of nanojet by simply shearing the micro particles particularly when the peak intensity lies inside the surface of micro-particle.

### 3.2 Manipulation using beam parameter

#### 3.2.1 Wavelength dependence of PNJ characteristics

The effect of excitation wavelength on the length and width of

PNJ is shown in Figure T.1.7 for a fixed size and refractive index of microsphere. As noted earlier, better confinement of PNJ is obtained for longer wavelength since for a fixed size of microsphere the size parameter reduces with increase in the wavelength.

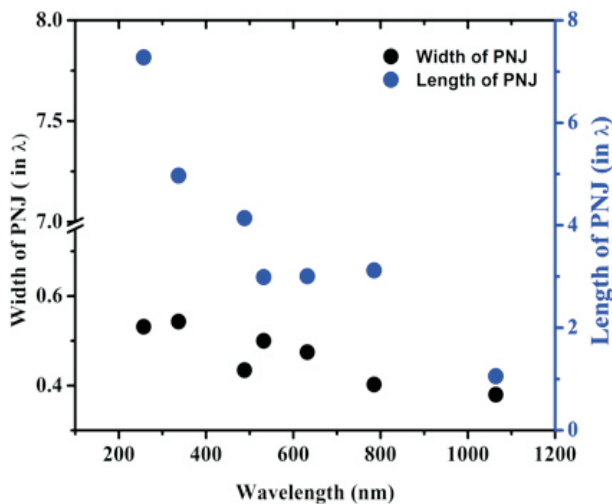


Fig. T.1.7: Wavelength dependence of length and width of PNJ generated by 3  $\mu\text{m}$  diameter microsphere. Refractive index of microsphere was taken as  $n_s = 1.45$  in air surrounding.

### 3.2.2 Manipulation of PNJ using wave front shaping

Change in illumination condition has been shown to have profound effect on the nanojet characteristics. Kim *et al.* [24] first demonstrated that by suitably introducing an optical component that can modify the amplitude and/or phase distributions of the incident beam, it is possible to tailor the PNJ characteristics over a wide range. Illuminating the microsphere with incident beam having converging (diverging) spherical wavefront leads to generation of highly localized (elongated) nanojet. This is easily achieved by suitably manipulating the position of microsphere placed in the optic axis under focused Gaussian beam illumination. Positive curvature imparted by the microsphere to the propagating beam adds the curvature of incident spherical wavefront resulting in shift of maximum intensity point in PNJ. This approach can be used for manipulating the working distance of nanojet. Using the focused Gaussian beam it is also possible to have off axis illumination of the microsphere. Effect of lateral shift in beam position with respect to the microsphere centre shows that it is possible to achieve angular tuning of emerging nanojet. Such non-collinear nanojets have applications in developing simple approach for efficient coupling to the slab waveguide and manipulation of nanoparticles in crowded environment.

### 3.2.3 Manipulation of PNJ using beam polarization

Polarization of the incident beam plays an important role in determining the strength of longitudinal component of field in the optical near field of the microsphere. Use of radially and azimuthally polarized beam along with the doughnut and Bessel beam profile have been used to generate PNJ with special characteristics [24]. The radially polarized beam when used with engineered microsphere having thick layer of opaque mask of varying cover ratio has been shown to generate nanojet with strong longitudinal field component. The high longitudinal component thus generated have applications in the field of optical super resolution imaging, Raman spectroscopy and particle acceleration.

## 4. Photonic nanojet applications

Owing to subwavelength confinement of light, PNJs have been explored for many interesting applications. Some of the important applications of PNJ are as follows:

### 4.1 Detection and localization of nanoparticle

In the original article on PNJ, Chen *et al.* [10] theoretically demonstrated that the nanoparticles moving in the transverse direction through the field of nanojet leads to a significant enhancement in backscattering of light. This was utilized by Heifetz *et al.* to experimentally demonstrate detection and localization of a 20-nm diameter gold nanoparticle with a sub-diffraction transverse spatial resolution [39]. Theoretical simulation using perturbation approach shows that gold nanoparticles as small as 2 nm in diameter produce sufficient backscattering enhancement ( $\sim 34\text{dB}$ ) compared to microsphere alone. The backscattering signal was found to increase linearly over a wide range of diameter (2 - 60 nm) of interest. The backscattered power for smaller sized nanoparticles has been found to be proportional to the volume of nanoparticle in contrast to the volume square dependence that is expected for Rayleigh scattering. This has a potential bio-photonics application in detection of nanoparticles attached to the membranes of living cells in an aqueous environment.

### 4.2 Enhancement of Raman scattering

High local intensity in the photonic nanojets generated by dielectric microsphere has been used experimentally by several groups to enhance the Raman signal from different substrates. An order of magnitude intense Raman signal was reported by making use of self-assembled silica and polystyrene microspheres on silicon substrate [25]. We have carried out systematic investigation of effect of size of microsphere and refractive index contrast between microsphere and sample on the Raman enhancement factor.



The experimental data show that enhancement factor not only varies with the size of microsphere but also strongly depends on the refractive index contrast between the sample and microsphere. Higher the refractive index of sample vis-a-vis the microsphere, larger is the enhancement. The enhancement factor falls rapidly as the sample refractive index approaches that of the microsphere. The simulation results show that maximum enhancement is obtained when the peak intensity in PNJ is near the sample-microsphere interface. As the refractive index contrast between the sample and microsphere decreases, the length of nanojet gets elongated resulting in reduced enhancement factor. We have further shown that by decoupling the excitation and collection, it is possible to achieve an order of magnitude enhancement of Raman signal even from the samples having lower refractive where PNJ are quite elongated [40]. The use of microsphere assisted enhancement of Raman signal can therefore be a useful aid in label free analysis of the biological samples. Apart from being a cost effective approach PNJ assisted enhancement of Raman signal can also be coupled with other approaches like CARS and SERS etc. for a synergistic enhancement of signal. Chang *et al.* [41] have reported Raman enhancement factor of  $\sim 3.6 \times 10^{10}$  by making use of photonic nanojet assisted Marangoni convection to increase the turnover of analytes in SERS hotspots in liquid environment. The combined PNJ-SERS based Raman spectroscopy may therefore be a potentially useful approach for alleviating the problems associated with reproducibility of signal in SERS.

#### 4.3 Ultrahigh density optical data storage

Heat-assisted magnetic recording is capable of writing data in excess of 1 Tb/in<sup>2</sup> density by temporarily heating the area of a single bit on the hard disk to its Curie temperature using a near field transducer. Challener *et al.* have explored use of PNJ for coupling of light into the near field transducer [42]. While the theoretical simulation shows that nanojet-illuminated pits having lateral dimensions of only 50 nm × 80 nm can give up to 27 dB better contrast than using a conventional lens based system, experimental results on scaled up model show that high density optical storage with individual bit stored in  $\sim 0.025\lambda^2$ , can be robustly detected. To put this perspective it should be noted here that the current commercial Blu-Ray disks have pit size of about  $\lambda/4$  and track pitch of  $\lambda/1.25$ .

#### 4.4 Maskless nano-patterning and nanolithography

PNJ generated by self-assembled planar structure of silica microsphere upon illumination with a 400 nm centred ultraviolet (UV) broad band light source was used successfully by Wu *et al.* [29] to demonstrate maskless lithography with a feature size down to 250 nm. Maskless

lithography using microsphere allows nano-writing at even at lower fluence and provides better control of the hole or pillar diameter by varying the exposure time. McLeod and Arnold [30] have shown nano-lithography using photonic nano jet generated by optically trapped submicron size polystyrene microspheres. Microsphere was trapped using 532 nm continuous-wave laser Bessel beam and simultaneously illuminated with a 355 nm pulsed Gaussian beam to generate the nanojet which was used for writing on the substrate. A resolution of 102 nm ( $\sim \lambda/3.5$ ) and 130 nm ( $\lambda/2.7$ ), was achieved using the optically trapped microsphere of 0.5  $\mu\text{m}$  and 0.8  $\mu\text{m}$  sized polystyrene microspheres.

#### 4.5 Near field trapping of nano particles

Optical forces on metallic nanoparticles induced by a photonic nanojet were first calculated by Cui *et al.* to demonstrate stable trapping of metallic sub-wavelength nanoparticle using the optical forces acting on it in the electromagnetic field of PNJ [43]. Force acting on the particles was shown to be sensitive to polarization and reverses the sign upon changing polarization. Optical forces on dielectric particles near subwavelength slits illuminated by a PNJ have been investigated by Valdivia-Valero *et al.* [44]. Numerical simulation has also been carried out to show that the hook shaped curve nanojet generated by asymmetric micro cuboid can be used for nanoparticle manipulation along a specific path thereby allowing better manoeuvring of particles around the obstacles [45]. The exquisite control over the particle's motion offered by photonic hook may enable sorting and manipulation of particle in microfluidic devices and 'lab-on-a-chip' platforms without the need for multiple trapping beam. On the experimental front trapping and manipulation of nanoparticles using the standing wave formed by two counter propagating photonic nanojets was demonstrated by Wang *et al.* [46]. More recently trapping of cells and macromolecules has also been reported using photonic nanojet array [47].

#### 4.6 Low loss optical waveguide

Remote addressing of the optical nano devices is important for selective and high throughput delivery of signal at desired port. Photonic nanojet induced modes in chain of optical microsphere has been shown to be an experimentally efficient approach for low loss ( $< 0.08$  dB/ microsphere) delivery of visible light at distal end of the microsphere chain [48]. PNJ induced coupling offers significant advantages over the commonly used coupling technique based on whispering gallery mode. This is because the formation of nanojet is a non-resonant phenomenon and has been shown to be relatively insensitive to the deformation and surface



corrugations in the microspheres. Therefore, polydispersity in the microsphere diameters do not adversely affect the waveguiding characteristics.

#### 4.7 Super-resolution optical imaging

The ability to confine electromagnetic field to sub-diffraction spot size makes the photonic nanojet a good candidate for collecting information from confined region of sub-wavelength size. This follows the principle of reciprocity consideration which states that reverse process of collecting optical information from sub diffraction region should also be possible by just time reversal. It is therefore expected that microsphere can help relay the nearfields in a similar way as in collection mode NSOM to break the diffraction limit. Indeed the microsphere based nanoscopy has been demonstrated to achieve deep subwavelength resolution down to  $\sim \lambda/17$  [32]. Super resolution imaging with microspheres has also been demonstrated in aqueous environments suitable for imaging of biological samples using high refractive index microsphere. The choice of microsphere refractive index is guided by the fact that increase in refractive index of background liquid medium causes the nanojet peak to shift in the far field and needs to be compensated for bringing it closer to the surface for effectively relaying the high spatial frequency information. Imaging of sub-cellular structures in biological samples like centrioles, mitochondria and chromosomes etc. [49] and single adenovirus [50] have also been demonstrated using microsphere nanoscope. While the microsphere nanoscopy provides wide field image of the features under the microsphere it is desirable for many practical applications to precisely control the positioning of microspheres over the sample. Krivitsky *et al.* [33] demonstrated that attaching a glass micropipette near equatorial plane of microsphere has minimal effect on its PNJ characteristics and used it for moving the particle to perform scanning over the sample area. It was followed by successful demonstration of super resolution imaging by using a microsphere mount on AFM cantilever for precise scanning over the sample [32]. Since the generation of nanojet is a non-resonance phenomenon, microsphere nanoscopy can also be performed using white light. More recently, 3D cluster of material forming a metamaterial solid immersion lens was explored for possibility of generating periodic near field nanojets that may allow nanoscopy and nano patterning with resolution down to  $\sim 15$ -30 nm [51].

#### 4.8 Single molecule spectroscopy

Fluorescence correlation spectroscopy (FCS) is one of the most powerful single molecule detection techniques for analysis of molecules at extremely low concentration. However, the basic principle of FCS requires that the

concentration of molecules and the excitation volumes should be such that only few molecules are simultaneously present in the focal volume. This requires a complicated optical instrumentation which is limited by diffraction criteria as far as the detection volume is concerned. PNJ generated by dielectric microspheres under focused Gaussian illumination were used by Gerard *et al.* [27,28] to achieve optical confinement of the detection volume below the diffraction limit. While the reduced observation volume allows measurements at significantly higher concentration, using planner array of microsphere it is also possible to create multi-focus FCS with photonic nanojet arrays to enable single molecule sensitivity at pico-molar concentration. More recently, PNJ has also been coupled with surface enhanced Raman spectroscopy (SERS) to utilize Marangoni convection set in by the nanojet to enhance the turnover of analytes into the hotspot region [35]. This approach allows detection and chemical analysis of the analytes with a single molecule sensitivity and nanometer scale spatial resolution in a label free manner.

#### References

- [1] B. Huang, M. Bates and X. Zhuang, *Annu. Rev. Biochem.* 78, 993–1016 (2009).
- [2] R. Heintzmann and G. Ficz, *Methods Cell Biol.* 114, 525-544 (2013).
- [3] A. G. Godin, B. Lounis and L. Cognet, *Biophys. J.* 107, 1777–1784 (2014).
- [4] S. W. Hell and J. Wichmann, *Opt. Lett.* 19, 780-782 (1994).
- [5] E. Betzig, G. H. Patterson and H. F. Hess, *Science* 313, 1642–1645 (2006).
- [6] M. J. Rust, M. Bates and X. Zhuang, *Nat. Methods*, 3, 793–795 (2006).
- [7] M. G. Gustafsson, *J Microsc.* 198, 82-87 (2000).
- [8] J. W. P. Hsu, *Mat. Sci. Eng. R: Reports* 33, 1–50 (2001).
- [9] F. J. Garcia-Vidal, L. Martin-Moreno, T. W. Ebbesen and L. Kuipers, *Rev. Mod. Phys.* 82, 729–787 (2010).
- [10] Z. G. Chen, A. Taflove, and V. Backman, *Opt. Exp.* 12, 1214-1220 (2004).
- [11] J. P. Barton, D. R. Alexander and S. A. Schaub, *J. Appl. Phys.* 64, 1632-1639 (1988).
- [12] S. Lecler, Y. Takakura and P. Meyrueis, *Opt. Lett.* 30, 2641-2643 (2005).
- [13] S. C. Kong, A. Taflove and V. Backman, *Opt. Exp.* 17, 3722-3731 (2009).
- [14] C. Liu, *Phys. Lett. A* 376, 1856-1860 (2012).

- [15] T. Jalali and D. Erni, *J. Mod. Opt.* 61, 1069-1076 (2014).
- [16] Y. E. Geints, I. V. Minin, E. K. Panina, A.A. Zemlyanov and O. V. Minin, *Opt. Quant. Electron.* 49, 118 (2017).
- [17] S.C. Kong, A. V. Sahakian, A. Heifetz, A. Taflove, and V. Backman, *Appl. Phys. Lett.* 92, 211102 (2008).
- [18] P. Ferrand, J. Wenger, A. Devilez, M. Pianta, B. Stout *et al.*, *Opt. Exp.* 16, 6930 (2008).
- [19] I. Mahariq, H. Kurt, *J. Opt. Soc. Am. B* 32, 1022 (2015).
- [20] I. Mahariq, V.N. Astratov, H. Kurt, *J. Opt. Soc. Am. B* 33, 535 (2015).
- [21] B. Lukyanchuk, R. P. Domínguez, I. Minin, O. Minin and Z. Wang, *Opt. Mat. Exp.* 7, 1820 (2017).
- [22] P. Wu, J. Li, K. Wei and W. Yue, *Appl. Phys. Exp.* 8, 112001 (2015).
- [23] H. S. Patel, P. K. Kushwaha and M. K. Swami, *Opt. Comm.* 415, 140-145 (2018).
- [24] M. Kim, T. Scharf, S. Mühligh, C. Rockstuhl and H. P. Herzig *Opt. Exp.* 19, 10206-10220 (2011).
- [25] K. J. Yi, H. Wang, Y. F. Lu, and Z. Y. Yang, *J. Appl. Phys.* 101, 063528 (2007).
- [26] J. F. Cardenas, *J. Raman Spectrosc.* 44, 540-543 (2013).
- [27] D. Gerard, A. Devilez, H. Aouani, B. Stout, N. Bonod, J. Wenger, E. Popov, and H. Rigneault, *J. Opt. Soc. Am. B* 26, 1473-1478 (2009).
- [28] D. Gerard, J. Wenger, A. Devilez, D. Gachet, B. Stout, N. Bonod, E. Popov, and H. Rigneault, *Opt. Express* 16, 15297-15303 (2008).
- [29] W. Wu, A. Katsnelson, O.G. Memis, H. Mohseni, *Nanotech.* 18, 485302 (2007).
- [30] E. McLeod, C.B. Arnold, *Nat. Nanotechnol.* 3, 413-417 (2008).
- [31] J. Kim, K. Cho, I. Kim, W.M. Kim, T.S. Lee, K. Lee, *Appl. Phys. Express* 5, 025201 (2012).
- [32] Z. Wang, W. Guo, L. Li, B. Luk'yanchuk, A. Khan, Z. Liu, Z. Chen, M. Hong, *Nature Commun.* 2, 218 (2011).
- [33] L.A. Krivitsky, J.J. Wang, Z. Wang, B. Lukyanchuk, *Sci. Rep.* 3, 3501 (2013).
- [34] I. Minin, O. Minin and Y. E. Geints *Ann. Phys.* 527, 491-497 (2015).
- [35] N. Eti, I. H. Giden, Z. Hayran, B. Rezaei and H. Kurt, *J. Mod. Opt.* 64, 1566-1577 (2017).
- [36] H. Ding, L. Dai and C. Yan, *Chin. Opt. Lett.* 8, 706-708 (2010).
- [37] M. J. Riedl in *Optical design fundamentals for infrared systems*, SPIE Press Bellingham, USA, 2<sup>nd</sup> Edition (2001).
- [38] C. Liu, *Physica E* 64, 23-28 (2014).
- [39] A. Heifetz, S. Kong, A.V. Sahakian, A. Taflove and V. Backman, *J. Comp. Theo. Nanosc.* 6, 1979-1992 (2009).
- [40] H. S. Patel, P. K. Kushwaha and M. K. Swami, *J. Appl. Phys.* 123, 023102 (2018).
- [41] T. W. Chang, X. Wang, A. Mahigir, G. Veronis, G. L. Liu, and M. R. Gartia, *ACS Sens.* 2, 1133 (2017).
- [42] W. A. Challener And A. V. Itagi, in *Modern Aspects of Electrochemistry* 44, M. Schlesinger (Ed.), Pp53-111, Springer, New York (2009).
- [43] X. Cui, D. Erni and C. Hafner *Opt. Exp.* 16, 13560-13568 (2008).
- [44] F. J. Valdivia-Valero, M. Nieto-Vesperinas *Opt. Comm.* 294, 351-360 (2013).
- [45] L. Yue, O. V. Minin, Z. Wang, J. N. Monks, A. S. Shalin, and I. V. Minin, *Opt. Lett.* 43, 771-774 (2018).
- [46] H. Wang, X. Wu, and D. Shen, *Opt. Lett.* 41, 1652-1655 (2016).
- [47] Y. Li, H. Xin, X. Liu, Y. Zhang, H. Lei and B. Li, *ACS Nano*, 10, 5800-5808 (2016).
- [48] K. W. Allen, A. Darafsheh, F. Abolmaali, N. Mojaverian, N. I. Limberopoulos, A. Lupu, and V. N. Astratov, *Appl. Phys. Lett.* 105, 021112 (2014).
- [49] H. Yang, N. Moullan, J. Auwerx, and M. A. M. Gijs, *Small* 10, 1712-1718 (2014).
- [50] L. Li, W. Guo, Y. Yan, S. Lee and T. Wang, *Light: Sci. Appl.* 2, e104 (2013).
- [51] W. Fan, B. Yan, Z. Wang, and L. Wu, *Sci. Adv.* 2, e1600901 (2016).